Sensitivity analysis of frequency response functions for load resistance of piezoelectric energy harvesters

Rabie Aloui, Walid Larbi, Mnaouar Chouchane

Sensitivity Analysis of Frequency Response Functions for Load Resistance of Piezoelectric Energy Harvesters

Rabie Aloui[1(✉)], Walid Larbi[2], and Mnaouar Chouchane[1]

[1] National Engineering School of Monastir (ENIM),
Avenue Ibn Jazzar, 5019 Monastir, Tunisia
{rabie.aloui,mnaouar.chouchane}@enim.rnu.tn
[2] Structural Mechanics and Coupled Systems Laboratory (LMSSC),
Conservatoire National des Arts et Metiers (CNAM),
292, rue Saint-Martin, 75141 Paris Cedex 03, France
walid.larbi@cnam.fr

Abstract. Piezoelectric energy harvesting from ambient energy sources, particularly vibrations, has attracted considerable interest throughout the last decade. Sensitivity analysis is a promising method used for many engineering problems to assess input-output systems based on vibration. In this paper, the formulation of first order sensitivity (FOS) of complex Frequency Response Functions (FRFs) is developed to evaluate the output responses of piezoelectric energy harvesters. The adapted approach for the FOS is the finite difference method, which consists in computing an approximation of the first derivation. Furthermore, the main goal is to study the influence of the variation of the load resistance from the short circuit (load resistance tends to zero) to open circuit (load resistance tends to the infinity) conditions on the tip displacement and the voltage FRFs of a Bimorph Piezoelectric Energy Harvester (BPEH). The determination of FRFs of the harvester are derived using Finite Element Modelling for a bimorph piezoelectric cantilever beam based on Euler-Bernoulli theory, which is composed of an aluminum substrate covered by two PZT-5A layers. The results show a high sensitivity of the FRFs of the BPEH to the load resistance at the natural frequencies. For each excitation frequency, the sensitivity near the resonance frequencies decreases from the short circuit conditions to the open circuit conditions.

Keywords: Sensitivity analysis · Vibration · Energy harvesting
Piezoelectric materials · Finite element method

1 Introduction

Sensitivity analysis of dynamic structures and mechatronic systems is very helpful in solving many engineering problems, such as: parametric identification problems, structural optimization, model updating problems and others (Lasecka-Plura and Lewandowski 2014), especially, for vibration energy harvesting devices using piezoelectric materials, which has been extensively studied over the past decade (Li et al.

2014). Several studies focused on modeling a multilayer cantilever beam with one, two or multi-piezoelectric layers used for vibration energy harvesting (Erturk and Inman 2011; Paknejad et al. 2016).

Two main approaches have been used by researchers for modeling piezoelectric energy harvesters are: (i) The analytical distributed parameter model (Erturk and Inman 2008, 2011) in which, the beam is modeled by a second-order partial differential equation in terms of beam tip displacement. (ii) The finite element model derived by De Marqui Junior et al. (2009) for an unimorph energy harvester plates, and a bimorph energy harvester cantilever beam (Amini et al. 2015). This formulation uses a standard discretization of beam layers, providing models with less restrictive assumptions, and takes into account the global electrical variables.

Since the first approach is limited to basic models, the finite element modeling is applied in this paper to determine the sensitivity of the frequency response functions (de Lima et al. 2010; Lasecka-Plura and Lewandowski 2014) of the bimorph piezoelectric energy harvester for the load resistance. The finite element equations of electromechanical problems are first presented. Then, the variational formulation of a laminated piezoelectric beam is developed for a Bimorph Piezoelectric Energy Harvester (BPEH) to determine the mechanical and electrical output FRFs. For the first order sensitivity analysis, the finite difference approach is applied to study the influence of the load resistance on the voltage and tip displacement FRFs.

2 Finite Element Modeling of the Energy Harvester

The finite element formulation of elastic structure with bonded piezoelectric patches proposed in (Thomas et al. 2009; Larbi et al. 2014) is used. The governing finite element equations of the dumped electromechanical problem can be expressed as:

$$\boldsymbol{M}_m\ddot{\boldsymbol{U}}(t)+\boldsymbol{C}_m\dot{\boldsymbol{U}}(t)+\boldsymbol{K}_m\boldsymbol{U}(t)+\boldsymbol{K}_c\boldsymbol{V}(t)=\boldsymbol{F}(t) \tag{1}$$

$$\boldsymbol{K}_e\boldsymbol{V}(t)-\boldsymbol{K}_c^T\boldsymbol{U}(t)=\boldsymbol{Q}(t) \tag{2}$$

where $\boldsymbol{M}_m$ is the global $(N\times N)$ mass matrix, $\boldsymbol{K}_m$ is the global $(N\times N)$ stiffness matrix, $\boldsymbol{C}_m$ is the global $(N\times N)$ damping matrix and $\boldsymbol{K}_c$ is the global electromechanical coupling matrix $(N\times P)$, $\boldsymbol{K}_e$ is the diagonal global $(P\times P)$ capacitance matrix, $\boldsymbol{F}(t)=\boldsymbol{F}e^{j\omega t}$ is the global $(N\times 1)$ vector of mechanical forces, $\boldsymbol{Q}(t)=\boldsymbol{Q}e^{j\omega t}$ is the global $(P\times 1)$ vector of electric charge outputs,$\boldsymbol{U}(t)=\boldsymbol{U}e^{j\omega t}$ is the global $(N\times 1)$ vector of mechanical coordinates and $\boldsymbol{V}(t)=\boldsymbol{V}e^{j\omega t}$ is the global $(P\times 1)$ vector of voltage outputs. Here, N and P respectively, are the number of mechanical degrees of freedom and the number of piezoelectric elements. The global mechanical damping matrix $\boldsymbol{C}_m$ is assumed a linear combination of the mass and stiffness matrices:

$$\boldsymbol{C}_m=\alpha\boldsymbol{M}_m+\beta\boldsymbol{K}_m \tag{3}$$

where α and β are the proportionality constants which are typically determined experimentally using at least two modal damping associated to two different natural frequencies.

Equation (1) corresponds to the mechanical equation of motion with electrical coupling, and a forcing vector $\boldsymbol{F}(t)$. Whereas Eq. (2) corresponds to the electrical circuit equation with a mechanical coupling term. In this paper, the harvested energy is dissipated through a resistive load R. Using Ohm's law, the following additional equation relates the voltage vector $\boldsymbol{V}$ and the charge vector $\boldsymbol{Q}$:

$$\boldsymbol{V}(t) = -R\dot{\boldsymbol{Q}}(t) \tag{4}$$

Considering in particular the finite element formulation of a laminated beam with a total of K layers including P piezoelectric layers, which is excited under sinusoidal base motion. Three mechanical degrees of freedom per node are used $\left(u, w, \theta \approx -\frac{\partial w_{rel}}{\partial x}\right)$. The piezoelectric layers of the cantilever beam are poled in the thickness direction with an electrical field applied parallel to this polarization. Such a configuration is characterized in particular by the electromechanical coupling between the axial strain ε_1 and the transverse electrical field E_3(Thomas et al. 2009). Furthermore, the reduced law behavior of a thin piezoelectric layer is written as follows:

$$\sigma_1 = \bar{c}_{11}\varepsilon_1 - \bar{e}_{31}E_3 \tag{5}$$

$$D_3 = \bar{e}_{31}\varepsilon_1 + \bar{\epsilon}_{33}E_3 \tag{6}$$

where $\sigma_1, \varepsilon_1, E_3$ and D_3 are respective the normal stress, normal strain, electric field and electric displacement, $\bar{c}_{11}$ is the elastic modulus, $\bar{e}_{31}$ is the piezoelectric coupling coefficient and $\bar{\epsilon}_{33}$ is the permittivity at constant strain. The variational formulation, in this case, is defined as follows:

$$\sum_{k=1}^{K}\int_{\Omega^k}\rho^k(\ddot{u}_x\delta u_x + \ddot{u}_z\delta u_z)d\Omega + \sum_{k=1}^{K}\int_{\Omega^k}\bar{c}_{11}^k\varepsilon_1\delta\varepsilon_1 d\Omega + \sum_{p=1}^{P}\frac{V^{(p)}}{h^{(p)}}\int_{\Omega^{(p)}}\bar{e}_{31}^{(p)}\delta\varepsilon_1 d\Omega = 0 \tag{7}$$

$$-\sum_{p=1}^{P}\frac{\delta V^{(p)}}{h^{(p)}}\int_{\Omega^{(p)}}\bar{e}_{31}^{(p)}\varepsilon_1 d\Omega + \sum_{p=1}^{P}\delta V^{(p)}C^{(p)}V^{(p)} = \sum_{p=1}^{P}\delta V^{(p)}Q^{(p)} \tag{8}$$

where ρ^k and Ω^k are the mass density and the domain occupied by the kth layer, $C^{(p)} = \frac{S^{(p)}}{h^{(p)}}\bar{\epsilon}_{33}^{(p)}$ is the capacity of the pth piezoceramic layer, where $S^{(p)}$ and $h^{(p)}$ are respectively the active surface and the thickness of the pth piezoceramic layer. The mechanical displacements u_x and u_z are defined as follow:

$$u_x(x,z,t) = u(x,t) - z\theta(x,t) \tag{9}$$

$$u_z(x,z,t) = w(x,t) = w_b(t) + w_{rel}(x,t) \tag{10}$$

where $w_b(t) = W_b e^{j\omega t}$ is the base displacement and $w_{rel}(x,t)$ is the relative displacement (for clamped-free beam).

The various terms appearing in the variational formulation in Eqs. (7) and (8) are now successively discussed.

- The kinetic energy variation is:

$$\sum_{k=1}^{K} \int_{\Omega^k} \rho^k (\ddot{u}_x \delta u_x + \ddot{u}_z \delta u_z) d\Omega \Rightarrow \delta \boldsymbol{U}^T \boldsymbol{M}_m \ddot{\boldsymbol{U}} - \delta \boldsymbol{U}^T \boldsymbol{F} \tag{11}$$

  where $\boldsymbol{F}$ is the inertial forcing vector due to base excitation which can be expressed as an effective mass vector $\boldsymbol{m}^*$ multiplied by the base acceleration (De Marqui et al. 2009) as follows:

$$\sum_{k=1}^{K} \int_{\Omega^k} \rho^k \delta w_{rel} \ddot{w}_b d\Omega \Rightarrow -\delta \boldsymbol{U}^T \boldsymbol{m}^* \ddot{w}_b = -\delta \boldsymbol{U}^T \boldsymbol{F} \tag{12}$$

- The mechanical contribution to the internal energy variation is:

$$\sum_{k=1}^{K} \int_{\Omega^k} \overline{c}_{11}^k \varepsilon_1 \delta \varepsilon_1 d\Omega \Rightarrow \delta \boldsymbol{U}^T \boldsymbol{K}_m \boldsymbol{U} \tag{13}$$

- The piezoelectric contributions to the internal energy variation, related to the direct and inverse effect, are given in the following equations.

$$\sum_{p=1}^{P} \frac{V^{(p)}}{h^{(p)}} \int_{\Omega^{(p)}} \overline{e}_{31}^{(p)} \delta \varepsilon_1 d\Omega \Rightarrow \delta \boldsymbol{U}^T \boldsymbol{K}_c \boldsymbol{V} \tag{14}$$

$$\sum_{k=1}^{P} \frac{\delta V^{(p)}}{h^{(p)}} \int_{\Omega^{(p)}} \overline{e}_{31}^{(p)} \varepsilon_1 d\Omega \Rightarrow \delta \boldsymbol{V}^T \boldsymbol{K}_c \boldsymbol{U} \tag{15}$$

- The electrical contribution to the internal energy variation is:

$$\sum_{p=1}^{P} \delta V^{(p)} C^{(p)} V^{(p)} \Rightarrow \delta \boldsymbol{V}^T \boldsymbol{K}_e \boldsymbol{V}. \tag{16}$$

3 Finite Element Modeling of a BPEH

In this section, the system matrices used in Eqs. (1) and (2) are derived using the finite element formulation of a bimorph piezoelectric vibration energy harvester excited by base motion. The harvester consists in an Euler Bernoulli beam composed of two layers of PZT-5A (piezoelectric material) bonded to an aluminum substrate (elastic material) as shown in Fig. 1. Thus, the total number of layers is equal to 3 ($K = 3$) the number of piezoelectric elements is equal to 2 ($P = 2$).

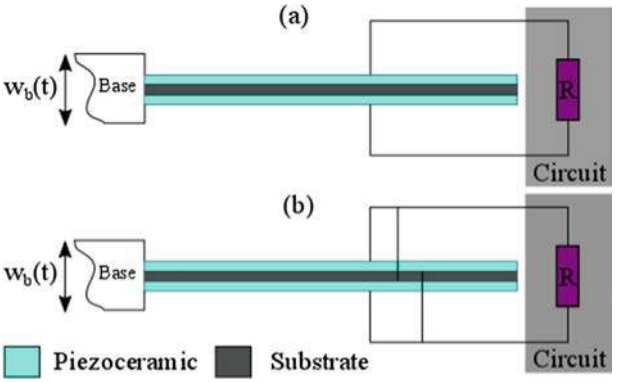

Fig. 1. Cantilever piezoelectric energy harvester configurations under base excitation: (a) bimorph (series connection) and (b) bimorph (parallel connection)

The electrical degrees of freedom associated to the two piezoelectric layers are the voltage vector $\boldsymbol{V}$ and charge vector $\boldsymbol{Q}$ defined as follows:

$$\boldsymbol{V} = \begin{pmatrix} V^{(1)} \\ V^{(2)} \end{pmatrix};\ \boldsymbol{Q} = \begin{pmatrix} Q^{(1)} \\ Q^{(2)} \end{pmatrix} \tag{17}$$

Each piezoelectric layer is characterized by its capacity $C^{(p)}$ and the electromechanical coupling vector $\boldsymbol{K}_c^{(p)}$, $p = 1, 2$.

$$\boldsymbol{K}_e = diag\left(C^{(1)}, C^{(2)}\right);\ \boldsymbol{K}_c = \begin{pmatrix} \boldsymbol{K}_c^{(1)} & \boldsymbol{K}_c^{(2)} \end{pmatrix} \tag{18}$$

3.1 Equivalent Representation of the Series and the Parallel Connection Cases of a BPEH

The equivalent representation of the finite element electromechanical equations of a BPEH for the series and the parallel connections is very useful to predict the electrical output responses across the resistor (in the circuit). For this purpose, the equivalent terms of the equivalent representation are obtained first.

The two-piezoceramic layers are assumed to be identical (same material, same dimensions). It is therefore reasonable to assume that both of them have the same capacity $\left(C^{(1)} = C^{(2)} = C\right)$ and generate the same output voltage so that $\left(V^{(1)} = V^{(2)} = V\right)$ and $\left(Q^{(1)} = Q^{(2)} = Q\right)$ (De Marqui et al. Junior 2009). Therefore, the nodal forces related to the converse piezoelectric effect ($\boldsymbol{K}_c\boldsymbol{V}$) when a voltage V is applied to the electrodes are given by the following term:

$$\boldsymbol{K}_c\boldsymbol{V} = \boldsymbol{K}_c \begin{pmatrix} 1 \\ 1 \end{pmatrix} V = \tilde{\boldsymbol{K}}_c V \tag{19}$$

Where $\tilde{\boldsymbol{K}}_c = \boldsymbol{K}_c^{(1)} + \boldsymbol{K}_c^{(2)}$ is the apparent electromechanical coupling vector $(N \times 1)$. Furthermore, the resulting charge and voltage in the circuit of the BPEH are given in Table 1 for the series and parallel connections (Erturk and Inman 2011).

Table 1. The charge and voltage in the electrical circuit for series and parallel connection of the two piezoelectric layers with a resistance load

	Series connection	Parallel connection
Charge in the circuit	Q	$2Q$
Voltage in the circuit	2 V	V

After modifying Eqs. (1) and (2) and transforming then to the frequency domain using Laplace transform, the equivalent electromechanical equations of a BPEH become:

$$\left[-\omega^2 \boldsymbol{M}_m + j\omega \boldsymbol{C}_m + \boldsymbol{K}_m\right]\boldsymbol{U} + \boldsymbol{K}_c^{eq} V = \boldsymbol{F} \tag{20}$$

$$\left(j\omega C^{eq} + \frac{1}{R}\right) V - j\omega \boldsymbol{K}_c^{eqT} \boldsymbol{U} = 0 \tag{21}$$

where $\boldsymbol{K}_c^{eq}$ and C^{eq} are respectively the equivalent electromechanical coupling vector and the equivalent capacity of a BPEH, which are given in Table 2, V is the voltage across the load resistance (in the circuit).

Table 2. Equivalent electromechanical coupling and capacitance of a bimorph energy harvester for the series and the parallel connections of the piezoceramic layers

Terms	Series connection	Parallel connection
$\boldsymbol{K}_c^{eq}$	$\tilde{\boldsymbol{K}}_c/2$	$\tilde{\boldsymbol{K}}_c$
C^{eq}	$C/2$	$2C$

3.2 Frequency Response Functions

The FRFs are defined here as the response outputs of the BPEH (displacement, voltage, current, power) per base acceleration (in terms of the gravitational acceleration,g $= 9.81\ \mathrm{m/s^2}$). The equivalent expression for nodal displacements FRFs relative to the base excitation problem of the BPEH is:

$$\frac{\boldsymbol{U}}{-\omega^2 W_b} = \left(-\omega^2 \boldsymbol{M}_m + j\omega \boldsymbol{C}_m + \boldsymbol{K}_m + \frac{j\omega\, \boldsymbol{K}_c^{eq} \boldsymbol{K}_c^{eqT}}{\left(\frac{1}{R} + j\omega C^{eq}\right)}\right)^{-1} \boldsymbol{m}^* \tag{22}$$

For the mechanical response (vibration), only the transverse tip displacement FRF $(w_n/-\omega^2 W_b)$ is considered in this study (n is the total node number of standard discretization with linear elements).

The voltage FRF is obtained as a function of the nodal displacements FRFs.

$$\frac{V}{-\omega^2 W_b} = \frac{j\omega \boldsymbol{K}_c^{eqT}}{\left(\frac{1}{R} + j\omega C_p^{eq}\right)} \quad -\omega^2 \boldsymbol{M}_m + j\omega \boldsymbol{C}_m + \boldsymbol{K}_m + \frac{j\omega \boldsymbol{K}_c^{eq} \boldsymbol{K}_c^{eqT}}{\left(\frac{1}{R} + j\omega C^{eq}\right)}\Bigg)^{-1} \boldsymbol{m}^* \tag{23}$$

The current FRF and the power FRF are obtained from the voltage FRF as follows:

$$\frac{I}{-\omega^2 W_b} = \frac{1}{R}\left(\frac{V}{-\omega^2 W_b}\right); \; \frac{P}{-\omega^2 W_b} = \frac{1}{R}\left(\frac{V}{-\omega^2 W_b}\right)^2 \tag{24}$$

The four frequency response functions may be collected into a single vector defined as follows.

$$\boldsymbol{H} = \frac{1}{-\omega^2 W_b}\begin{bmatrix} w_n & V & I & P \end{bmatrix} \tag{25}$$

The global finite element matrices appearing in the FRFs establish the dependence of the response of the system on a set of parameters, and can be expressed in the following form.

$$\boldsymbol{H} = \boldsymbol{H}(\omega, \boldsymbol{p}) \tag{26}$$

Where $\boldsymbol{H}$ is the frequency response functions vector, $\boldsymbol{p}$ is a vector of parameters of the BPEH.

4 Finite Difference Approach to Sensitivity Analysis of FRFs

The finite difference method originates from a Taylor series expansion to approximate the first order sensitivity (FOS) and is undoubtedly the simplest method to implement. The FOS of the responses with respect to a given design parameter p_i, evaluated for a given set of values of the design parameters $\boldsymbol{p}^0$ is defined as the following partial forward derivative:

$$\left.\frac{\partial \boldsymbol{H}}{\partial p_i}\right|_{p_i^0} = \lim_{\Delta p_i \to 0} \frac{\boldsymbol{H}\left(\omega, p_i^0 + \Delta p_i\right) - \boldsymbol{H}\left(\omega, p_i^0\right)}{\Delta p_i} \tag{27}$$

where Δp_i is the parameter increment in the finite difference scheme, applied to the current value of the parameter p_i^0, while all other parameters are kept unchanged. The sensitivity of the response with respect to p_i can be numerically estimated by finite differences by successively computing the responses corresponding to $p_i = p_i^0$ and $p_i = p_i^0 + \Delta p_i$, and then calculating:

$$\left.\frac{\partial \boldsymbol{H}}{\partial p_i}\right|_{p_i^0} \approx \frac{\boldsymbol{H}\left(\omega, p_i^0 + \Delta p_i\right) - \boldsymbol{H}\left(\omega, p_i^0\right)}{\Delta p_i} \tag{28}$$

The accuracy of the sensitivity estimates depends on the choice of the value of the parameter increment Δp_i, which has to be small compared to the corresponding parameters p_i^0 but there are limitations due to numerical truncation. The choice of Δp_i is critical in the precision of the calculated derivatives. Therefore, Δp_i are chosen following rule proposed by Arruda and Santos (1993).

$$\Delta p_i = \min\{\|H(p_i)\|, \delta_i\} \tag{29}$$

where $||.||$ is the Euclidian norm of the output FRFs vector and δ_i is defined as:

$$\delta_i = \begin{cases} 10^{-1} & if \ \left|p_i^0\right| < 10^{-6} \\ 10^{-3}\left|p_i^0\right| & if \ \left|p_i^0\right| \geq 10^{-6} \end{cases} \tag{30}$$

In order to check the accuracy of the calculated first order sensitivity, an approximation of the FRF for the parameter $(p_i + \Delta p_i)$ is computed using the following formula:

$$\hat{\boldsymbol{H}}(\omega, p_i^0 + \Delta p_i) \approx \boldsymbol{H}(\omega, p_i^0) + \frac{\partial \boldsymbol{H}}{\partial p_i}\Delta p_i \tag{31}$$

where $\hat{\boldsymbol{H}}$ is the first order approximation of the output FRFs of the harvester.

5 Case Study

This section presents an example of a BPEH computed using the previous finite element model. The material properties and geometrical characteristics of the harvester used in this study are given in Table 3 (Erturk and Inman 2011). For the purpose of simulation, the coefficient for the first two modes are chosen to be $\zeta_1 = 0.010$ and $\zeta_2 = 0.012$, the constants α and β are computed using these coefficients. The computing of the first derivation using the finite difference approach consists in varying the nominal value of the parameter by 0.25% ($\Delta p_i = 0.25\%$ of p_i). The load resistance is mounted in series with the piezoelectric layers. The sensitivity analysis of the tip displacement and voltage FRFs of the BPEH for a load resistance R are presented here.

The analysis is carried out for the frequency range from 0 to 5000 Hz. The first three resonance frequencies of the BPEH for short-circuit ($R \rightarrow 0$) and open circuit ($R \rightarrow \infty$) conditions are given in Table 4. The effective electromechanical modal coupling factor $k_{eff,r}$ characterizes the energy exchange between the mechanical structure and the piezoelectric layers. It is usually defined, for the system rth mode, by:

Table 3. Material properties and geometrical characteristics of the reference PEH

Parameters		PZT-5A	Aluminum
L	Beam length (mm)	30	30
b	Beam width (mm)	5	5
h_p, h_s	Layers thickness	0.15	0.05
E_p, E_s	Young's modulus (GPa)	61	70
ρ_s, ρ_p	Mass density (kg/m^3)	7750	2700
$\bar{e}_{31}$	Piezoelectric constant (C/m^2)	−10.4	–
$\bar{\epsilon}_{33}$	Permittivity constant (nF/m)	13.3	–

$$k^2_{eff,r} = \frac{\left(f_r^{oc}\right)^2 - \left(f_r^{sc}\right)^2}{\left(f_r^{sc}\right)^2} \tag{32}$$

where f_r^{sc} and f_r^{oc} are, respectively, the short-circuit and open-circuit rth system natural frequencies.

Table 4. First three short-circuit and open-circuit natural frequencies of the BPEH, and the effective electromechanical coupling factor

Mode (r)	f_r^{sc} (Hz)	f_r^{oc} (Hz)	$k_{eff,r}$
1	181.1	191.1	0.0656
2	1159.8	1171.7	0.0206
3	3246.7	3258.0	0.007

The tip displacement and the voltage FRFs of the BPEH are given respectively in μm/g and V/g, and the resistance is expressed in Ω. Hence, the sensitivities relative to the load resistance are given respectively in μm/(g Ω) and V/(g Ω).

Figure 2 shows the first order sensitivity of the tip displacement FRF of the harvester with respect to the electrical load resistance R. Sensitivity analysis is applied for three resistances 100 Ω, 10 kΩ and 100 kΩ. It can be observed that the peaks of the FOS curves occur at the natural frequencies and has low values, around 10^{-7} over a wide range of frequencies.

The enlarged views of the FOS of the vibration to the load resistance given in Fig. 2 are presented as response surfaces using load resistance as an additional axis, Fig. 3. The absolute value of the sensitivity in the vicinity of resonance frequencies decreases from the short circuit conditions $(R \to 0)$ to the open circuit conditions $(R \to \infty)$. The sensitivity of the tip displacement (vibration) to the load resistance has lower values in the vicinity of the second mode compared to that of the first mode.

The variation of the sensitivity of the tip displacement of the BPEH for load resistance at the fundamental short-circuit resonance frequency and at the fundamental open-circuit resonance frequency are shown in Fig. 4. It is worth to note that the sensitivity curves are not completely monotonic. It should also be noted that the sensitivity of the vibration to the load resistance at the short circuit excitation frequency always remains greater in absolute value than that at the open circuit excitation frequency.

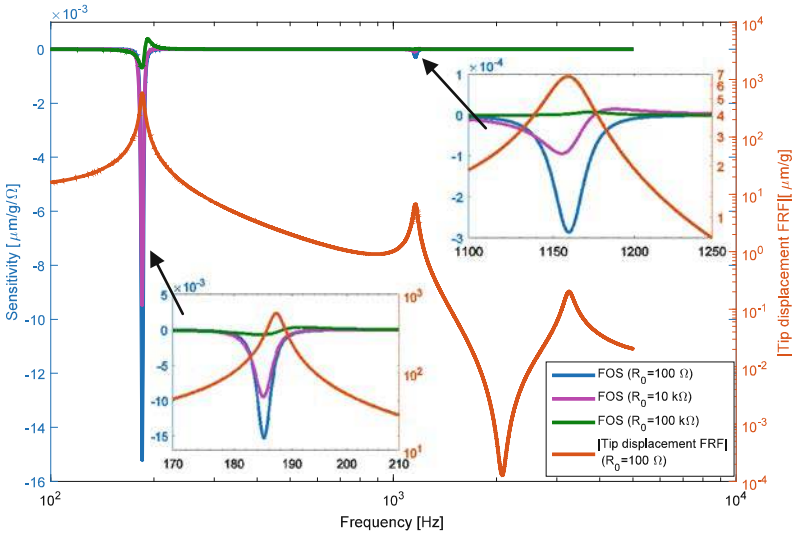

Fig. 2. First order sensitivity of tip displacement FRF modulus versus excitation frequency for three load resistances

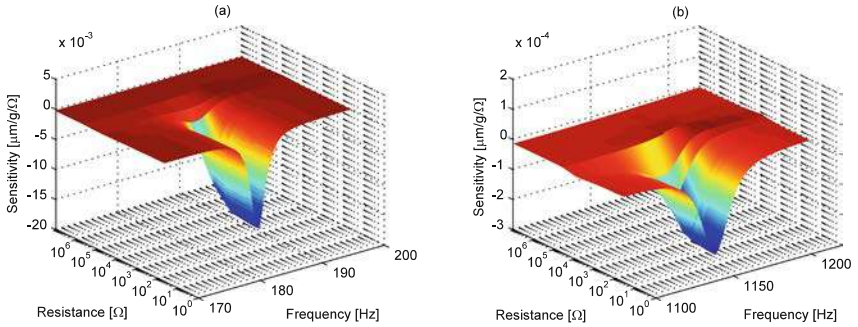

Fig. 3. First order sensitivity surface response of voltage FRF modulus versus excitation frequency and load resistance (a) in the vicinity of mode 1 (b) in the vicinity of mode 2

Figure 5 shows the first order sensitivity of the voltage FRF modulus versus the excitation frequency for three load resistances. We notice that the sensitivity for the load resistance is important in the vicinity of natural frequencies. The resistance value of 100 Ω has the largest sensitivities in the vicinity of the resonance frequencies, it is followed by the sensitivities of 10 kΩ, and finally the 100 kΩ sensitivity for each vibration mode.

Figure 6 shows that the sensitivity of the voltage output decreases when the resistance varies from the short circuit conditions to the open circuit conditions for all excitation frequencies. Furthermore, for each occurs of value of the resistance, the maximum value of sensitivity of voltage output matches the resonance frequency.

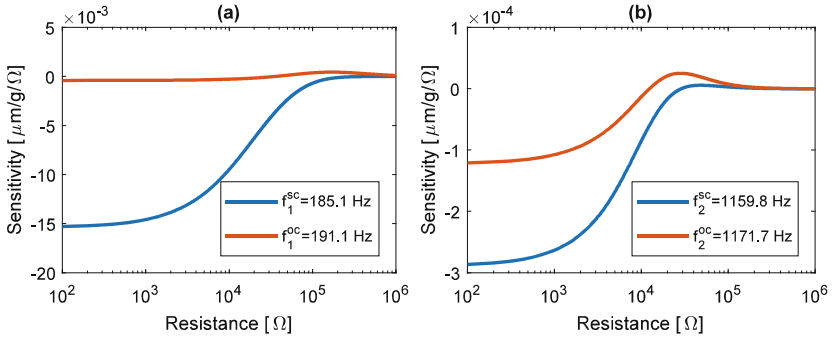

Fig. 4. Variation of the FOS of the tip displacement FRF to the load resistance versus load resistance for excitations at the short-circuit and the open-circuit resonance frequencies of: (a) mode 1 (b) mode 2

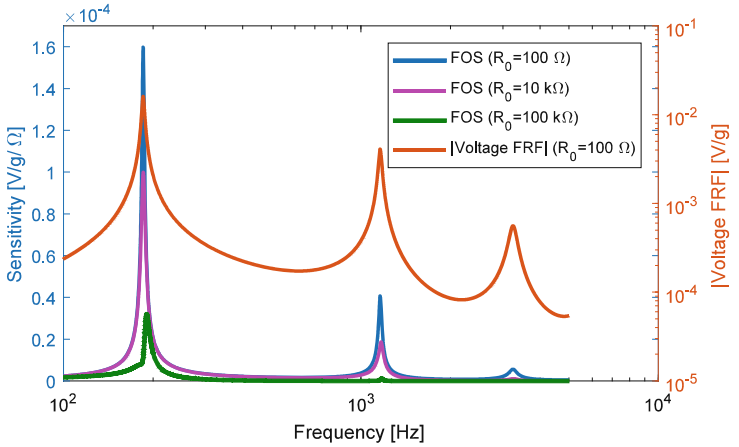

Fig. 5. First order sensitivity of voltage FRF modulus versus excitation frequency for three load resistance values

Therefore, the FOS of voltage FRF is significant at the natural frequencies and at low electrical load resistances (short circuit conditions).

Figure 7 shows the first order sensitivity of the voltage FRF modulus as a function of load resistance for excitations at the fundamental short-circuit and open-circuit resonance frequencies. For the first two modes, as the load resistance increases from the short-circuit to the open-circuit conditions, the sensitivity of the voltage FRF decreases monotonically. One can see clearly that the sensitivity of voltage FRF for the load resistance is more important for the short-circuit frequency excitation then the open-circuit frequency excitation for low resistance (short-circuit conditions). Both the sensitivities of the voltage FRF to the load resistance at the two fundamental resonance frequencies (short-circuit and open-circuit frequencies) have a very low value at the open-circuit condition.

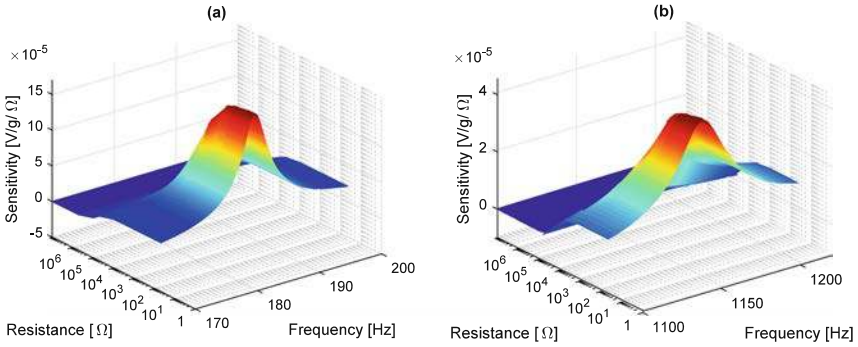

Fig. 6. First order sensitivity of modulus of Voltage FRF versus excitation frequency and load resistance (a) in the vicinity of mode 1 (b) in the vicinity of mode 2

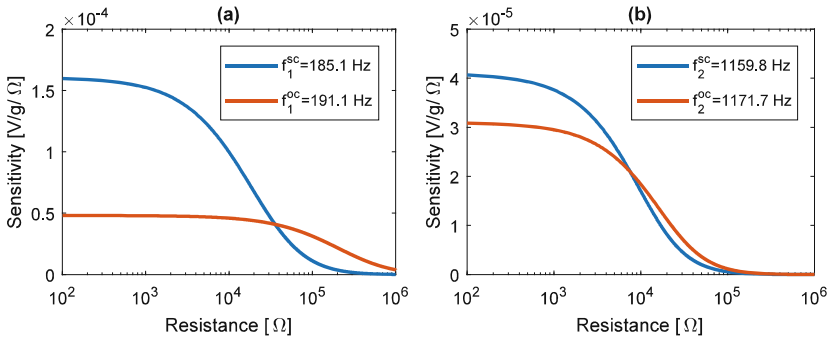

Fig. 7. Variation of the FOS of the voltage FRF for the load resistance versus load resistance for excitations at the short-circuit and the open-circuit resonance frequencies of: (a) mode 1 (b) mode 2

6 Conclusion

In this paper, the sensitivity analysis of frequency response functions has been considered. The finite difference approach has been used to approximate the first order sensitivity of tip displacement (vibration) and the voltage FRFs to a variation of the electrical load resistance of the harvester. The first order sensitivity analysis of the tip displacement and voltage FRFs of the BPEH have shown that the sensitivity to the load resistance is significant at the natural frequencies. Furthermore, the influence of the electrical load resistance variation for the vibration and voltage outputs is more important at the short circuit conditions than at the open circuit conditions. These results are very helpful to determine the optimal load resistance for an optimization study using the load resistance as a parameter.

References

Amini, Y., Emdad, H., Farid, M.: Finite element modeling of functionally graded piezoelectric harvesters. Compos. Struct. **129**, 165–176 (2015). https://doi.org/10.1016/j.compstruct.2015.04.011

Arruda, J.R.F., Santos, J.M.C.: Mechanical joint parameter estimation using frequency response functions and component mode synthesis. Mech. Syst. Signal Process. **7**, 493–508 (1993)

de Lima, A.M.G., Faria, A.W., Rade, D.A.: Sensitivity analysis of frequency response functions of composite sandwich plates containing viscoelastic layers. Compos. Struct. **92**, 364–376 (2010). https://doi.org/10.1016/j.compstruct.2009.08.017

De Marqui Jr., C., Erturk, A., Inman, D.J.: An electromechanical finite element model for piezoelectric energy harvester plates. J. Sound Vib. **327**, 9–25 (2009). https://doi.org/10.1016/j.jsv.2009.05.015

Erturk, A., Inman, D.J.: A distributed parameter electromechanical model for cantilevered piezoelectric energy harvesters. J. Vib. Acoust. **130**, 041002 (2008). https://doi.org/10.1115/1.2890402

Erturk, A., Inman, D.J.: Piezoelectric Energy Harvesting. Wiley, Chichester (2011)

Larbi, W., Deü, J.-F., Ohayon, R., Sampaio, R.: Coupled FEM/BEM for control of noise radiation and sound transmission using piezoelectric shunt damping. Appl. Acoust. **86**, 146–153 (2014). https://doi.org/10.1016/j.apacoust.2014.02.003

Lasecka-Plura, M., Lewandowski, R.: Design sensitivity analysis of frequency response functions and steady-state response for structures with viscoelastic dampers. Vib. Phys. Syst. **26** (2014)

Li, H., Tian, C., Deng, Z.D.: Energy harvesting from low frequency applications using piezoelectric materials. Appl. Phys. Rev. **1**, 041301 (2014). https://doi.org/10.1063/1.4900845

Paknejad, A., Rahimi, G., Farrokhabadi, A., Khatibi, M.M.: Analytical solution of piezoelectric energy harvester patch for various thin multilayer composite beams. Compos. Struct. **154**, 694–706 (2016). https://doi.org/10.1016/j.compstruct.2016.06.074

Thomas, O., Deü, J.-F., Ducarne, J.: Vibrations of an elastic structure with shunted piezoelectric patches: efficient finite element formulation and electromechanical coupling coefficients. Int. J. Numer. Methods Eng. **80**, 235–268 (2009). https://doi.org/10.1002/nme.2632